Influence of the Chemical Nature of the Support (Niobic Acid and Niobium Phosphate) on the Surface and Catalytic Properties of Supported CuO

A. Gervasini,*[,§,‡] P. Carniti,[§] S. Bennici,[§,#] and C. Messi[§]

Dipartimento di Chimica Fisica ed Elettrochimica and Centro di Eccellenza CIMAINA, Università degli Studi di Milano, via C. Golgi n. 19, 20133 Milano, Italy

Received October 20, 2006. Revised Manuscript Received December 22, 2006

The morphologic (N_2 adsorption and SEM), structural (XRD and FT−IR), redox (TPR/TPO cycles), acidic (TPD of 2-phenylethylamine), and surface (XPS) properties of supported CuO phases on niobic acid ($Nb_2O_5 \cdot nH_2O$, labeled as NBO) and niobium phosphate ($NbOPO_4$, labeled as NBP) materials were presented together with their catalytic properties toward the decomposition and reduction of the N_2O and NO species. An equilibrium adsorption method from copper acetate precursor was used to deposit the copper phase over the two niobium supports (about 8 wt % loading). The prevalent covalent, for NBO, or ionic, for NBP, character of the support materials strongly affected the electronic properties of the supported CuO phase, which was in nanosized aggregates in any case. The acidity of the Cu surfaces was high because of the presence of acid sites of the support (prevalent Brönsted acid sites) and those associated with dispersed metal species (Lewis acid sites). The CuO phase was better anchored on NBP than on NBO, as shown by the very limited migration of the CuO species on NBP following reducing and oxidizing thermal treatments. The CuO surfaces showed different catalytic performances toward the reactions of N_2O decomposition in inert and oxidant atmospheres and N_2O and NO reduction by ethene in a highly oxidant atmosphere. CuO over NBO was more active than that over NBP in any case, whereas the NBP support enhanced the reaction selectivity of the copper phase.

Introduction

The importance of dispersed CuO-based catalysts in the industrial chemistry (e.g., methanol synthesis, steam reforming, water−gas shift reactions)[1−5] and environmental chemistry processes (e.g., NO_x decomposition and reduction, CO oxidation)[6−10] has been well-assessed in the last decades. The catalytic performances of the supported CuO phases depend on the dimension of the aggregates and interfacial interaction with the support, besides the copper loading. In particular, for the reactions involving nitrogen oxides (N_2O, NO, and NO_2), the nanosized dimensions of the CuO aggregates and strong interaction with the support guarantee good performances in terms of activity and selectivity.[8,11−18]

Niobium compounds are actually considered important catalytic materials that find application as promoters, active phases, and supports of metals and metal oxides.[19−23] Among the various used Nb-containing materials, hydrated niobium pentoxide ($Nb_2O_5 \cdot nH_2O$), generally called niobic acid, and niobium phosphate ($NbOPO_4$) are unusual acidic solids[23−25] that are able to catalyze a variety of reactions, including

* Corresponding author. E-mail: antonella.gervasini@unimi.it.
§ Dipartimento di Chimica Fisica ed Elettrochimica, Università degli Studi di Milano.
‡ Centro di Eccellenza CIMAINA, Università degli Studi di Milano.
# Present address: IRCELYON, UMR5256 CNRS−Université LYON 1, 2 avenue Albert Einstein, 69626 Villeurbanne, France.

(1) Guerreiro, E. D.; Gorriz, O. F.; Rivarola, J. B.; Arrua, L. A. *Appl. Catal., A* **1997**, *165*, 259−271.
(2) Rao, R. S.; Walters, A. B.; Vannice, M. A. *J. Phys. Chem. B* **2005**, *109*, 2086−2092.
(3) Waugh, K. C. *Catal. Today* **1992**, *15*, 51−75.
(4) Bluhm, H.; Havecker, M.; Knop-Gericke, A.; Kleimenov, E.; Schlogl, R.; Teschner, D.; Bukhtiyarov, V. I.; Ogletree, D. F.; Salmeron, M. *J. Phys. Chem. B* **2004**, *108*, 14340−14347.
(5) Koryabkina, N. A.; Phatak, A. A.; Ruettinger, W. F.; Farrauto, R. J.; Ribeiro, F. H. *J. Catal.* **2003**, *217*, 233−239.
(6) Shimizu, K.; Maeshima, H.; Yoshida, H.; Satsuma, A.; Hattori, T. *Phys. Chem. Chem. Phys.* **2000**, *2*, 2435−2439.
(7) Dandekar, A.; Vannice, M. A. *Appl. Catal., B* **1999**, *22*, 179−200.
(8) Carniti, P.; Gervasini, A.; Modica, V. H.; Ravasio, N. *Appl. Catal., B* **2000**, *28*, 175−185.
(9) Morales, J.; Caballero, A.; Holgado, J. P.; Espinos, J. P.; Gonzalez-Elipe, A. R. *J. Phys. Chem. B* **2002**, *106*, 10185−10190.
(10) Pietrogiacomi, D.; Sannino, D.; Tuti, S.; Ciambelli, P.; Indovina, V.; Occhiuzzi, M.; Pepe, F. *Appl. Catal., B* **1999**, *21*, 141−150.
(11) Bennici, S.; Carniti, P.; Gervasini, A. *Catal. Lett.* **2004**, *98*, 187−194.
(12) Gervasini, A.; Manzoli, M.; Martra, G.; Ponti, A.; Ravasio, N.; Sordelli, L.; Zaccheria, F. *J. Phys. Chem. B* **2006**, *110*, 7851−7861.
(13) Márquez-Alvarez, C.; Rodríguez-Ramos, I.; Guerrero-Ruiz, A.; Haller, G. L.; Fernández-García, M. *J. Am. Chem. Soc.* **1997**, *119*, 2905−2914.
(14) Torre-Abreu, C.; Ribeiro, M. F.; Henriques, C.; Ribeiro, F. R. *Appl. Catal., B* **1997**, *11*, 383−401.
(15) Indovina, V.; Occhiuzzi, M.; Pietrogiacomi, D.; Tuti, S. *J. Phys. Chem. B* **1999**, *103*, 9967−9977.
(16) Bennici, S.; Gervasini, A. *Appl. Catal., B* **2006**, *62*, 336−344.
(17) Schwarz, J. A. *Chem. Rev.* **1995**, *95*, 477−510.
(18) Bennici, S.; Auroux, A.; Guimon, C.; Gervasini, A. *Chem. Mater.* **2006**, *18*, 3641- 3650.
(19) Tanabe, K.; Okazaki, S. *Appl. Catal., A* **1995**, *133*, 191−218.
(20) Tanabe, K. *Catal. Today* **2003**, *78*, 65−77.
(21) Nowak, L.; Ziolek, M. *Chem. Rev.* **1999**, *99*, 3603−3624.
(22) Ziolek, M. *Catal. Today* **2003**, *78*, 47−64.
(23) Florentino, A.; Cartraud, P.; Magnoux, P.; Guisnet, M. *Appl. Catal., A* **1992**, *89*, 143−153.
(24) Morais, M.; Torres, E. F.; Carmo, L. M. P. M.; Pastura, N. M. R.; Gonzalez, W. A.; dos Santos, A. C. B.; Lachter, E. R. *Catal. Today* **1996**, *28*, 17−21.
(25) Carniti, P.; Gervasini, A.; Biella, S.; Auroux, A. *Chem. Mater.* **2005**, *17*, 6128−6136.

10.1021/cm062503v CCC: $37.00
Published on Web 02/15/2007

hydrocarbon transformations, hydrations, dehydrations, and esterifications,[19,20,23,26] among others. Because of a high Tamman's temperature of the niobic acid and niobium phosphate materials, with the consequent absence of mobility of the surface atoms in a temperature range typical of catalytic reactions (473−873 K), they can also be attractive support materials.

The surface acid properties of supports play a key role in the interfacial interaction with the supported oxide phases.[12,16,27,28] Hydrated niobium pentoxide calcined at moderate temperatures (<573 K) has high acid character with Lewis and Bronsted sites ($H_o = -5.6$), whereas its acidity decays for higher calcination temperatures, becoming an almost neutral oxide after treatment at 873 K. Niobium phosphate has texture and acidic properties similar to niobic acid, but it has the advantage that it conserves these properties at higher temperatures.[21] Several examples of supported metal oxides over niobia can be found in the literature,[29−32] whereas, as far as the authors know, niobium phosphate has never been used as the support phase.

In this work, we have prepared and studied catalytic materials comprising CuO ionic oxide supported over niobic acid and niobium phosphate. The dispersion of CuO over niobic acid should give rise to a stable system possessing Lewis sites (cations of the ionic oxide) and Brönsted acid sites of the support covalent oxide.[33] The coupling of two prevalently ionic materials, CuO on niobium phosphate, is not very usual in catalysis because of the possibility of salt formation.[33] Because CuO consists of cations of large size (Cu(I) or Cu(II) species are about 0.75−1.50 Å) unable to enter the close packing of a niobium phosphate support, a fairly stable mixed structure can be formed. The structural, textural, surface, redox, and acid properties of the two systems were comparatively investigated. Moreover, on the basis of the known de-NO_x activity of copper oxide phases, reactions of decomposition and reduction of NO_x were chosen as test reactions to determine the catalytic properties of the supported CuO phases.

Experimental Section

Material Preparation. The as-received niobium pentaoxide hydrate (HY-340, AD/1079, CBMM) and niobium phosphate (ADF/26, CBMM), hereafter called NBO and NBP, respectively, were used as dispersing supports for the copper oxide phase. The copper deposition was performed over 10 g of each support by an equilibrium adsorption method dropping an aqueous copper acetate solution (230 mL, 0.05 M) into the slurry of the support in water (NBO or NBP in 120 mL) kept at 298 K and a pH value of 8, maintained by ammonia solution addition. The suspension was then kept under stirring for 24 h and filtered to obtain the solid. The filtered waters contained residual copper acetate, which was not adsorbed on the support. The residual copper concentration in the solution was determined by spectrophotometric analysis (Beckman DU 640; molar extinction coefficient: $\epsilon_{Cu(C_2H_3O_2)_2} = 22.92$ cm^2 mmol^{-1}). Eventually, the solid was dried (393 K for 12 h) and calcined (773 K in air for 4 h). The suitability of the calcination temperature to remove all the organic content was checked comparing the thermogravimetric profiles (TGA) of the dried and calcined samples in the 323−1073 K (15 K min^{-1}) collected under flowing air. The obtained samples were labeled as Cu/NBO and Cu/NBP. NBO and NBP supports were calcined (773 K in air for 4 h) too and comparatively analyzed with the CuO catalysts.

Material Characterization. Scanning electron micrographs (SEM) were obtained on a LEO 1430 instrument operating at 30 kV. The samples were analyzed under a high vacuum (about 1×10^{-7} mbar) after gold coating.

Surface area (BET) and porosity were determined by conventional N_2 adsorption at 77 K using a Sorptomatic 1900 version instrument from Carlo Erba. Prior to the analysis, the calcined supports and Cu-samples (0.2−0.3 g) were outgassed at 623 K for 16 h. Pore volume distribution was calculated from the desorption branch of the isotherm using the Barrett Joyner Halenda (BJH) model equation.[34]

XRD diffraction analyses on the calcined NBO and NBP powders as well as Cu catalysts were carried out in a Philips PW1710 vertical goniometric diffractometer using Ni-filtered Cu$K_{\alpha 1}$ radiation ($\lambda =$ 1.54178 Å). The chamber rotated around the sample at 1° (2θ) min^{-1}; the range of investigation was 5−80° (2θ).

FT−IR spectra were measured on a BioRad FTS-40 spectrophotometer using KBr pellets. The as-received and calcined NBO and NBP supports and Cu catalysts were recorded at r.t. (room temperature) in the 4000−400 cm^{-1} range with 100 scans s^{-1} and a resolution of 4 cm^{-1}.

XPS analyses of the Cu catalysts were carried out with a VG Scientific ESCALAB 200 R_electron spectrometer using Al Kα monochromatized exciting radiation (1486.6 eV). The residual pressure in the analysis chamber was around 1×10^{-9} mbar. All binding energy (BE) measurements were corrected for charging effects with reference to the C 1s peak of the adventitious carbon (284.6 eV). BE values were estimated with an accuracy of ±0.2 eV. The collected data were analyzed using a nonlinear Shirley-type background.[35] The signal intensities were measured by integration of the detected peaks; for each species, correction by the Scofield sensitivity factors was performed.[36]

Conventional temperature-programmed reduction experiments (TPR) were performed on the calcined NBO and NBP supports and Cu catalysts using a TPD/R/O-1100 instrument (CE Instruments). In any case, weighted samples of about 0.05 g were used. The amount of CuO in the sample (ca. 60 μmol) was suitable to obtain values[37] for K and P of 100 s and 50 K, respectively. The samples were initially pretreated in flowing air (45 mL min^{-1}) at 623 K for 1 h. After being cooled to 323 K, the H_2/Ar (5.1% v/v) reducing mixture flowed through the sample at 15 mL min^{-1} while the temperature was increased from 323 to 1223 K at constant rate

(26) Da Silva, J. C. G.; Folgueras-Domínguez, S.; Dos Santos, A. C. B. *J. Mater. Sci. Lett.* **1999**, *18*, 197−200.
(27) Chen, Y.; Zhang, L. *Catal. Lett.* **1992**, *12*, 51−62.
(28) *Oxide Based Materials: New Sources, Novel Phases, New Applications* (Studies in Surface Science and Catalysis); Proceedings of the Third International Workshop on Oxide Based Materials: New Sources, Novel Phases, New Applications, Societá del Casino Sociale, Como, Italy, Sept 13−16, 2004; Colella, C., Coluccia, S., Gamba, A., Eds.; Elsevier Science: Amsterdam, 2005; Vol. 155.
(29) Chary, K. V. R.; Seela, K. K.; Sagar, G. V.; Sreedhar, B. *J. Phys. Chem. B* **2004**, *108*, 658−663.
(30) Martín, C.; Solana, G.; Malet, P.; Rives, V. *Catal. Today* **2003**, *78*, 365−376.
(31) Petre, A. L.; Perdigón-Melón, J. A.; Gervasini, A.; Auroux, A. *Catal. Today* **2003**, *78*, 377−386.
(32) Cherian, M.; Rao, M. S.; Deo, G. *Catal. Today* **2003**, *78*, 397−409.
(33) Busca, G. *Phys. Chem. Chem. Phys.* **1999**, *1*, 723−736.
(34) Barrett, E. P.; Joyner, L. G.; Halenda, P. *J. Am. Chem. Soc.* **1951**, *73*, 373- 380.
(35) Shirley, D. A. *Phys. Rev. B* **1972**, *5*, 4709−4714.
(36) Scofield, J. H.; *J. Electron Spectrosc. Relat. Phenom.* **1976**, *8*, 129−137.
(37) Malet, P.; Caballero, A. *J. Chem. Soc., Faraday Trans. 1* **1988**, *184*, 2369−2375.

Table 1. Chemical and Morphological Characteristics of the Samples

	Cu loading		microstructure		
sample	wt %	D_{Cu}[a,b] ($atom_{Cu}$ nm^{-2})	surface srea (m^2 g^{-1})	porosity (cm^3 g^{-1})	pore radius[c] (nm)
NBO			63.53	0.153	4.8
Cu/NBO	7.91	16.04	46.74	0.120	5.1
NBP			84.52	0.272	6.4
Cu/NBP	7.95	10.73	70.21	0.246	7.0

[a] Copper density calculated as amount of Cu per unit surface. [b] Theoretical monolayer values: Cu/NBO, 8 wt%; Cu/NBP, 10 wt %. [c] Calculated by the Gurvitsh rule.

of 8 K min^{-1}. Redox cycles on the Cu catalysts were realized using the TPD/R/O-1100 instrument as well, carrying out in sequence a first temperature-programmed reduction (TPR-1) on the oxidized sample, followed by temperature-programmed oxidation (TPO-1) analysis and repeating the cycle two times (TPR-1/TPO-1/TPR-2/TPO-2/TPR-3). Before the redox cycle, the sample was pretreated in flowing air as detailed above. The H_2/Ar mixture flowed at 15 mL min^{-1} when the temperature increased from 323 to 800 K (8 K min^{-1}). TPO run was carried out on the reduced sample cooled at 323 K in a H_2/Ar flow. After Ar purge (10 mL min^{-1}), the O_2/He (1.1% v/v) oxidizing mixture flowed at 15 mL min^{-1} with experimental conditions, in terms of temperature increasing and range, similar to those used for TPR analysis. The H_2 or O_2 consumption was detected by a thermal conductivity detector (TCD). Peak areas were calibrated with pure H_2 or O_2 injections (Sapio, Italy; 6.0 purity) and, for H_2 consumption, with a thermal reduction of high-purity CuO wires.

The acidic properties of the calcined NBO and NBP supports and Cu catalysts were determined by 2-phenylethylamine (PEA) thermal desorption in a thermogravimetric apparatus (TGA 7 Perkin-Elmer). The calibration of temperature was performed by measuring the Curie transitions (T_C) of high-purity reference materials. Prior to the TGA analysis, the powder sample was outgassed (1.33×10^{-3} mbar) for 16 h at 623 K and then transferred to a glass cell into which liquid PEA (purity >99% from Fluka) was introduced under flowing N_2 until the powder was completely covered. The slurry rested at room temperature under flowing N_2 for 3 h. The excess nonadsorbed PEA was then removed by filtration; this operation was carried out under N_2 as well. The obtained saturated powder was loaded on the pan of the TGA (10−15 mg) and a two-step analysis was carried out, both under N_2 flowing at 30 mL min^{-1}. The first isothermal step was carried out at 323 K to remove the excess PEA condensed on the surface and it lasted up to constant mass (about 10 h). The second step was carried out at constant heating rate ($\beta = 10$ K min^{-1}) from 323 to 1173 K, to completely remove PEA from the surface. The total mass loss of PEA was determined by subtracting the final sample mass at 1123 K from the mass recorded at the end of the first isothermal step of the analysis. Assuming a 1:1 stoichiometry for the PEA adsorption on the acid site, we were able to determine the total number of sites of the surface. The PEA desorption curves have been reproduced, the number of acid sites of the surfaces could be estimated with an accuracy of ±5%. The derivative of the TGA curves (DTGA) gave the temperatures at which the maximum rate of PEA desorption occurred (T_{max}) from the acid sites of definite strength.

Catalytic Measurements. Catalytic tests of activity were performed in a continuous reaction line setup for reactions of reduction and decomposition of nitrogen oxides already described.[11,16,] Direct decomposition of N_2O in inert (He) or oxidant (O_2/He) atmospheres and reduction of N_2O and NO by C_2H_4 in a highly oxidant atmosphere were studied (feed concentration of the NO, N_2O, and C_2H_4 reagent species of 1500 and 15 000 ppm of O_2 with He as balance). The sample (0.3 g sieved as 45−60 mesh particles) was put into the quartz microreactor and, after in situ pretreatment (623 K in a 20% O_2/He stream for 4 h), worked at a fixed contact time of 0.360 s in the 573−873 K temperature range. An on-line FT−IR spectrophotometer (Bio-Rad with DTGS detector) was used for the analysis of the feed and reactor out streams quantifying the intensity of selected absorbance lines: NO (1876.0 cm^{-1}), N_2O (3493.2 cm^{-1}), C_2H_4 (951.4 cm^{-1}), CO (2086.5 cm^{-1}), and CO_2 (720.6 cm^{-1}).

Results and Discussion

Preparation. The copper deposition over the NBO and NBP supports was performed by the so-called equilibrium adsorption method[17] from aqueous solution containing the copper precursor salt. The separated solids by filtration were light blue (NBO) and light green (NBP) and the colors were maintained after calcination. Comparative analysis of the TGA analyses of dried and calcined Cu samples confirmed the complete removal of all the organic contents following the calcination procedure. Besided the mass losses observed at low temperatures (<373 K) that are due to water removal, important mass losses were observed around 473 and 530 K on dried Cu/NBO and Cu/NBP, respectively. The observed difference in the temperature values of organic removal and creation of the CuO phase could reflect the different interaction of copper with the oxide or phosphate surfaces.

The adopted operative conditions of Cu deposition (temperature and, in particular, pH of the slurry of the support and copper salt) guaranteed the almost complete Cu adsorption (around 99%) on the support surfaces. The obtained Cu loading was around 8 wt % (10 wt % in CuO) in any case (Table 1). The surfaces of NBO and NBP should be almost completely covered by copper, the calculated theoretical monolayer values[38] were 8 wt % for Cu/NBO and 10 wt % for Cu/NBP. This corresponded to values of copper surface density (D_{Cu}) of 11 and 16 $atom_{Cu}$ nm^{-2} for Cu/NBP and Cu/NBO, respectively.

The skeletal IR spectra of as-received and calcined NBO and NBP were consistent with those reported in the literature.[26,39−41] For the NBO samples, characteristic absorptions were observed at 994−960 cm^{-1} (stretching of short Nb═O bond of highly distorted NbO_6 octahedra) and at 629−583 cm^{-1} (symmetric and asymmetric stretching of a long Nb−O bond of distorted NbO_6 octahedra). On Cu/NBO, very reduced absorption in the 629−583 cm^{-1} range could be observed. Very similar IR spectra were observed for both

(38) Ries, H. E.; Laidler, K. J.; Innes, W. E.; Ciapetta, F. G.; Plank, C. J.; Selwood, P. W. In *Catalysis*: *Volume I Fundamental Principles (Part I)*; Emmett, P. H., Ed.; Reinhold Publishing: New York, 1954; p 258.
(39) Stranford, G. T.; Condiate, R. A. *J. Solid State Chem.* **1984**, *52*, 248−253.
(40) Armaroli, T.; Busca, G.; Carlini, C.; Giuttari, M.; Raspolli Galletti, A. M.; Sgrana, G. *J. Mol. Catal., A* **2000**, *151*, 233−243.
(41) Braga, V. S.; Dias, J. A.; Dias, S. C. L.; de Macero, J. L. *Chem. Mater.* **2005**, *17*, 690−695.

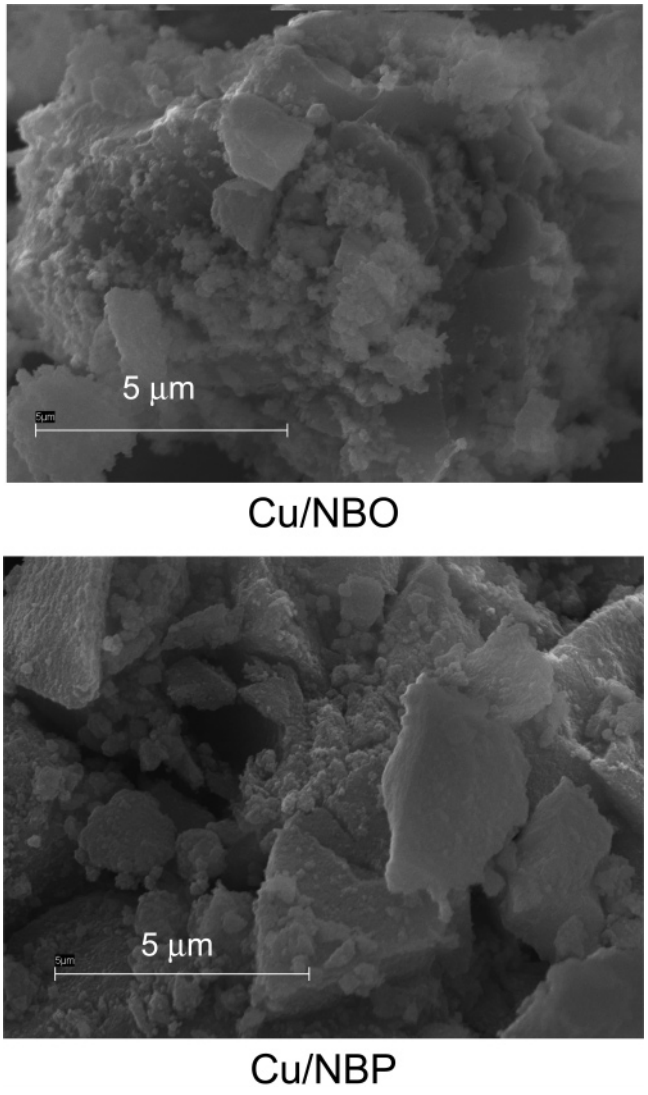

Figure 1. SEM micrographs of Cu/NBO and Cu/NBP surfaces.

as-received and calcined NBP. In addition to the bands of Nb−O stretching modes, an additional broad band located at 1020 cm^{-1} with a shoulder at 1100 cm^{-1} was observed, due to the O−P−O asymmetric stretching modes of phosphate or polyphosphate groups. At the high absorption frequencies, a broad asymmetrical band centered at 3400 cm^{-1} was observed with high intensity for the as-received NBO and NBP and with reduced intensity for the calcined NBO and NBP. On Cu/NBO sample, the high-frequency region was completely flat, whereas a very light decrease in intensity was observed on Cu/NBP compared with NBP. As the absorption corresponds to H-bonded surface OH stretching modes (i.e., Nb−OH retaining water), it can be inferred that copper preferentially bound to acidic OH groups when NBO is used as the support.

SEM micrographs of Figure 1 show the morphology of the Cu/NBO and Cu/NBP surfaces (Figure 1). Irregularly shaped particles were observed, comprising wider polyhedral blocks (support) and a non-agglomerated almost spherical phase (deposited metal). The presence of porosity is well evident for Cu/NBP, whereas it is more hidden for Cu/NBO.

Characterization. *XRD.* The X-ray diffraction patterns of the Cu catalysts and the parent calcined supports are

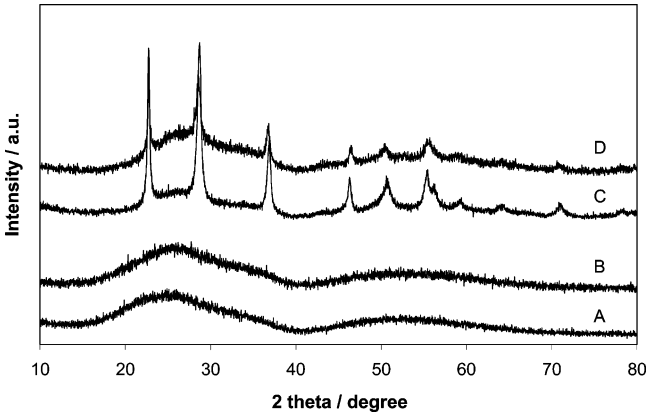

Figure 2. XRD patterns of the calcined (A) NBP, (B) Cu/NBP, (C) NBO, and (D) Cu/NBO.

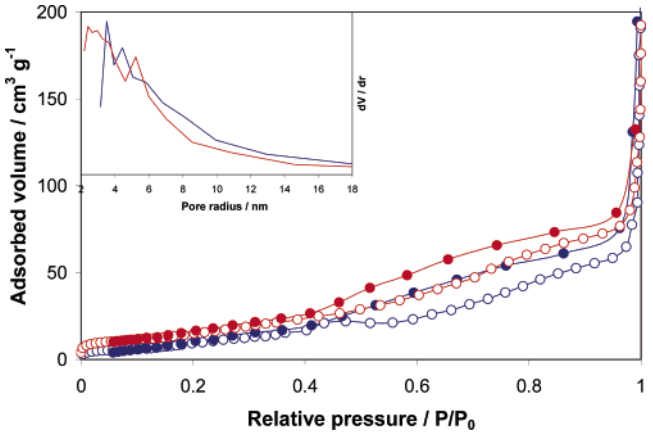

Figure 3. N_2 adsorption (open symbol) and desorption (filled symbol) isotherms and pore distribution plots (inset) of NBO (red) and Cu/NBO (blue).

shown in Figure 2. Typical diffractograms of amorphous materials were obtained for the NBP-containing samples, whereas XRD peaks of low-temperature niobia was clearly observed for the NBO containing samples (d = 3.92, 3.11, 2.44, 1.96, 1.80, 1.66, and 1.63 Å, corresponding to 22.73, 28.71, 36.9, 46.35, 50.7, 55.5, and 56.0° 2θ). The peak positions suggest the presence of the TT-phase of niobia, in agreement with that reported by Ko and Weissman.[43] The niobia aggregate dimensions evaluated by the Sherrer equation gave values around 80 nm. The diffractogramm of Cu/NBO as well as that of Cu/NBP (parts B and C of Figure 2) did not show any characteristic peaks of the crystalline CuO phase; the most intense line of CuO, corresponding to the (111) plane at d = 2.52 Å, should appear at 35.55° 2θ. The absence of XRD peaks of CuO indicates that the metal phase was present in a highly dispersed amorphous state on both the supports with size of the CuO aggregates less than 10 nm.

Texture. Surface area and porosity of the calcined supports and Cu catalysts have been studied by collecting N_2 adsorption and desorption isotherms. As shown in Figure 3, NBO and Cu/NBO couple, and in Figure 4, NBP and Cu/NBP couple, the copper deposition on NBO and NBP did not alter the shape of the isotherms of the relevant support.

(42) Onfroy, T.; Clet, G.; Houalla, M. *J. Phys. Chem B* **2005**, *109*, 14588−14594.
(43) Ko, E. I.; Weissman, J. G. *Catal. Today* **1990**, *8*, 27−36.

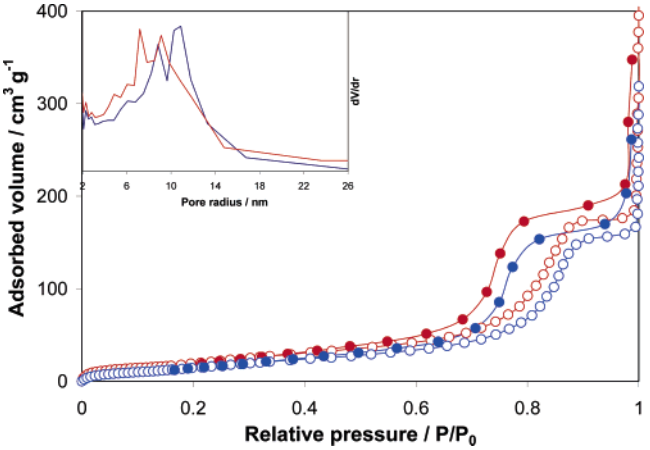

Figure 4. N_2 adsorption (open symbol) and desorption (filled symbol) isotherms and pore distribution plots (inset) of NBP (red) and Cu/NBP (blue) samples.

Table 2. Surface Composition Obtained from XPS Results

	BE Cu 2p$_{3/2}$ (eV)		atomic ratios between components			
sample	satellite	main peak	Nb/O	Cu/O	Cu/P	Cu/Nb
Cu/NBO	943.2	934.0	0.40	0.08		0.20
	941.0	932.1				
Cu/NBP	943.3	934.8	0.23	0.066	0.40	0.28
	940.3	932.2				

In any case, both the adsorption and desorption branches of the support isotherms lie over those of the relevant Cu catalysts. As a consequence, the obtained values of surface area and pore volume of NBO and NBP are higher than those of Cu catalysts (Table 1). This indicated that the two supports were covered by the CuO phase with smaller surface areas. Comparing the obtained surface areas and porosities of NBO and NBP with those recently reported in the literature for the same samples,[25] one can notice different values. This is due to the different activation treatments of the samples that were calcined at 673 K for the work of ref 25 and have been calcined at higher temperature (773 K) for the present investigation (see the Experimental Section).

The shape of the isotherms of the NBO-containing samples is different from those containing NBP, especially as far as the hysteresis shapes are concerned. Isotherms of Figure 3 seem to have type H3 hysteresis (according with IUPAC classification) that is typical of solids consisting of aggregates forming slit-shaped pores with nonuniform size and/or shape. On the contrary, isotherms of Figure 4 seem to have type H1 hysteresis, which is characteristic of solids consisting of particles crossed by nearly cylindrical channels with uniform size and shape. The profiles of pore distribution of the two support−catalyst couples (insets of Figures 3 and 4) show the same trend. A little but significant shift toward higher pore radius for the Cu catalysts compared with the relevant supports can be noticed.

XPS. The qualitative and quantitative surface analysis of Cu catalysts was focused on niobium (Nb 3d$_{5/2}$, 207.0−207.3 eV), oxygen (O 1s, 530.1−530.9 eV), copper (Cu 2p$_{3/2}$, 932.1−934.8 eV), and phosphorus (P 2p, 133.3 eV). The oxygen content of the NBO and NBP surfaces is very similar (atomic values of 57.3 and 59.5% for Cu/NBO and Cu/NBP, respectively) whereas the copper content (atomic values of 4.4 and 3.9% for Cu/NBO and Cu/NBP, respectively), and

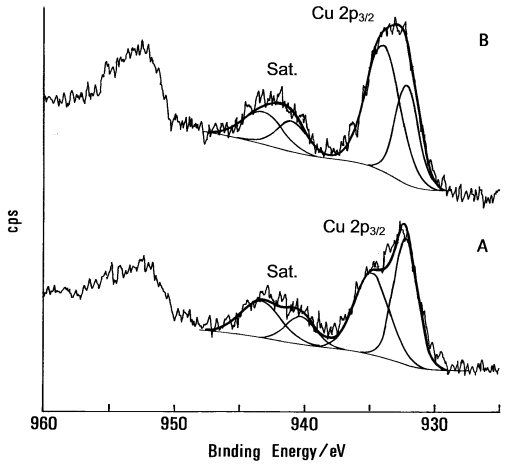

Figure 5. X-ray photoelectron spectra (XPS) of Cu 2p core level of the (A) Cu/NBP and (B) Cu/NBO.

in particular, the niobium content (atomic values of 22.9 and 13.9% for Cu/NBO and Cu/NBP, respectively) are very different. For both the Cu catalysts, the surface composition is reported as Nb/O, Cu/O, Cu/P, and Cu/Nb (Table 2). In both the cases, the measured ratios are in excellent agreement with the bulk ratios that can be calculated from the Cu catalyst composition (Table 1), indicating that the totality of copper has been deposited as small particles on both the surfaces.

The Nb 3d$_{5/2}$ binding energy values around 207 eV for both the Cu catalysts well fit the corresponding binding energy of niobia,[44] indicating the single presence of Nb^{5+} species without any modification following copper deposition. The electronic situation of copper on the two supports was complex, as shown by the XP spectra reported in Figure 5. Broad and convoluted XPS bands around 934 eV (Cu 2p$_{3/2}$), along with shakeup satellite peaks (942 eV) that clearly indicate the presence of Cu^{2+} species (Table 2), could be observed. The shape and position of the XPS bands are in agreement with analogous observations on various supported copper systems.[6,29,45,46] The XPS bands were decomposed into two contributions. The high-energy contribution of the main XPS bands, typical of CuO, was at 934.0 eV for Cu/NBO, whereas it was shifted toward higher energy, 934.8 eV, for Cu/NBP. The shift can be indicative of a strong charge transfer from the copper species toward the NPB support.[12,47] The low-energy contribution of the main bands (around 932 eV, typical of Cu^+ species)[47] could be indicative of Cu(I) presence. The reduced copper species could be originally present at the catalyst surfaces (formed during the preparation/calcinations steps) or they could derive from partial photoreduction of the Cu(II) species by X-ray beam during data collection. From a quantitative point of view, the relative intensity of low-energy component of XPS band at 932 eV did not show a significant difference between the two catalysts.

(44) Moulder, J. F.; Stickle, W. F.; Sobol, P. E.; Bomben, K. D. *Handbook of XPS*; Perkin-Elmer: Eden Prairie, MN, 1992.
(45) Espinos, J. P.; Morales, J.; Barranco, A.; Caballero, A.; Holgado, J. P.; Gonzalez-Elipe, A. R. *J. Phys. Chem. B* **2002**, *106*, 6921−6929.
(46) Indovina, V.; Occhiuzzi, M.; Pietrogiacomi, D.; Tuti, S. *J. Phys. Chem. B* **1999**, *103*, 9967−9977.
(47) Auroux, A.; Gervasini, A.; Guimon, C. *J. Phys. Chem. B* **1999**, *103*, 7195−7205.

Table 3. Redox Behavior of the Copper Phase from TPR/TPO Experiments

		T (K)			reduction	
sample	experiment	T_{on}	T_{max}	T_{end}	(μmol$_{H_2}$ g^{-1})	(%)
Cu/NBO	TPR-1	433	540 580	687	1253	101
	TPR-2	418	460 503	531	1245	100
	TPR-3	418	462 503	531	1130	92
	TPO[a]	375	435 570	639	n.d.[b]	
Cu/NBP	TPR-1	511	619	676	1142	92
	TPR-2	515	587	641	1114	90
	TPR-3	515	581	641	1114	90
	TPO[a]	376	455 615	678	n.d.[b]	

[a] Average parameters for the different collected TPO runs. [b] Not determined.

Redox Properties. First, on the two Cu-containing samples and relevant supports, conventional TPR runs were carried out up to 1223 K to study the reducibilty of the CuO and Nb phases. Reduction peaks were observed in two distinct ranges of temperature: 423−723 and 930−1173 K. From a comparison of the TPR profiles of the catalyst−support couples, it was possible to doubtless assign to CuO reduction the low-temperature peaks. Concerning the high-temperature peaks, both NBO and Cu/NBO gave a similar signal (shape and intensity) starting at 1050 K with the maximum at a temperature higher than 1143 K (it was difficult to individuate T_{max} with precision because we reached the limit of the analysis), assigned to niobium reduction. It is known that Nb_2O_5 yields an intense reduction peak around 1100 K that accounts for about 50% reduction (Nb^{5+} to Nb^{4+}).[30,48,49] TPR spectrum of Cu/NBP showed a well-defined symmetrical signal starting at 930 K with a maximum at 1080 K, whereas a completely flat line was obtained for NBP. This indicated that the high-temperature peak could be assigned to that part of copper not reduced at low temperature. In fact, integration of the TPR peak of Cu/NBP in the 511−676 K range gave only 92% of CuO reduction (Table 3); the remaining part of copper necessitated a much higher temperature to be reduced. During copper deposition on NBP, intermetallic compounds could be formed in analogy with copper−tin−phosphorus alloys, the well-known phosphor bronzes.

Second, the redox properties of the dispersed CuO phases were investigated realizing various cycles of temperature-programmed reductions and oxidations up to 800 K (corresponding to sample temperature of 780 K), to rule out reactions involving the support (in particular for NBO) and to avoid aggregation of the copper phase. The ability of working in a completely reversible redox cycle is requested to CuO by a variety of reactions, in particular, reductions, oxidations, dehydrogenations.[2,50,51] The shape and characteristic parameters (i.e., temperature of maximum reduction/oxidation) of the reduction/oxidation profiles are indicative of the properties of the reducible phases.[1,52] Moreover, when supported phases are concerned, significant information on the interaction with the support can be obtained, as well.

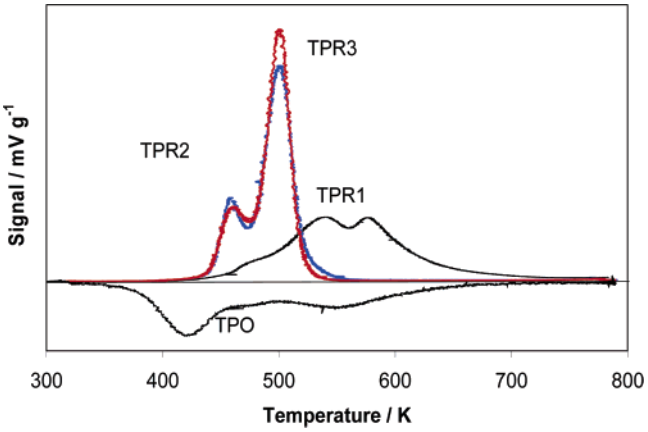

Figure 6. Redox cycles of Cu/NBO. Profiles of reduction (TPR1, black; TPR2, blue; and TPR3, red) and oxidation (TPO) at programmed temperature (8 K min^{-1}). A single TPO profile is reported; the other TPO profiles, collected after each TPR run, were all superposed.

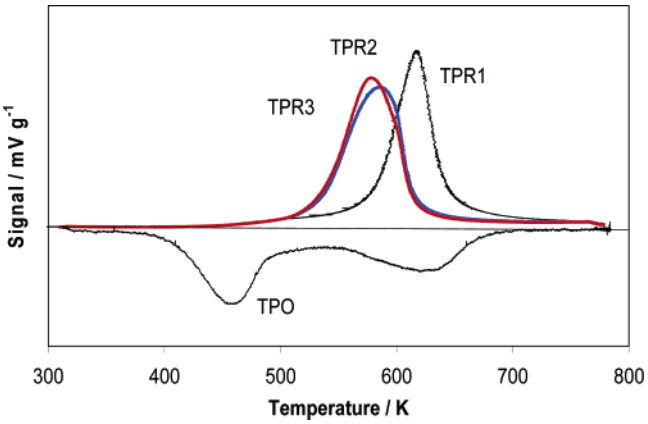

Figure 7. Redox cycles of Cu/NBP. Profiles of reduction (TPR1, black; TPR2, blue; and TPR3, red) and oxidation (TPO) at programmed temperature (8 K min^{-1}). A single TPO profile has been reported; the other TPO profiles, collected after each TPR run, were all superposed.

CuO is known to be an easily reducible phase with the possibility to work in a reversible redox cycle.[1,11,53] Table 3 summarizes the most significant results, in terms of onset, maximum, and end temperatures (T_{on}, T_{max}, and T_{end}, respectively) of the reduction and oxidation processes (TPR-1, TPR-2, TPR-3, and TPO) and the extent of CuO reduction calculated on the basis of hydrogen consumption in the different runs. A very broad and wide reduction peak (peak width of 254 K) in which two maxima (540 and 580 K) could be individuated was obtained in the first TPR run (TPR-1) for Cu/NBO (Figure 6). A completely different TPR-1 profile was obtained for Cu/NBP. A unique, quite symmetrical peak centered at 619 K with a width of 165 K was collected (Figure 7). The position of the peaks (T_{max} values) for both of the catalysts are compatible with the presence of small and well-dispersed CuO species in interaction with the support.[1,11,29,53,54] The deep differences in the shape of the TPR-1 profiles between Cu/NBO and Cu/NBP

(48) Nowak, I.; Kilos, B.; Ziolek, M.; Lewandowska, A. *Catal. Today* **2003**, *78*, 487−498.
(49) Ziolek, M.; Nowak, I. *Catal. Today* **2003**, *78*, 543−553.
(50) Agrell, J.; Birgersson, H.; Boutonnet, M.; Melian-Cabrera, I.; Navarro, R. M.; Fierro, J. L. G. *J. Catal.* **2003**, *219*, 389−403.
(51) Agrell, J.; Birgersson, H.; Boutonnet, M.; Melian-Cabrera, I.; Navarro, R. M.; Fierro, J. L. G. *J. Catal.* **2003**, *219*, 389−403.
(52) Fadoni, M.; Lucarelli, L. In *Adsorption and its Applications in Industry and Environmental Protection (Studies in Surface Science and Catalysis)*; Dabrowski, A., Ed.; Elsevier Science: Amsterdam, 1999; Vol. 120(A), Chapter 6.
(53) Bennici, S.; Gervasini, A.; Ravasio, N.; Zaccheria, F. *J. Phys. Chem. B* **2003**, *107*, 5168−5176.
(54) Córdoba, G.; Viniegra, M.; Fierro, J. L. G.; Padilla, J.; Arroyo, R. *J. Solid State Chem.* **1998**, *138*, 1−6.

suggest very different distribution of the CuO species on NBO and NBP surfaces. The percent of reduction was total for Cu/NBO and lower for Cu/NBP (as discussed above, Table 3). The higher T_{max} value of the TPR-1 peak of Cu/NBP than Cu/NBO could suggest the presence of larger CuO aggregates, even if XRD was not able to detect them or a higher metal oxide−support interaction. Oxidation by TPO of the reduced samples showed profiles with shapes that did not differ between each other in a remarkable way (Figures 6 and 7). In any case, the reoxidation of the Cu phases involved a two-step process; two peaks could be individuated whose T_{max} values differed appreciably between Cu/NBO and Cu/NBP. Higher T_{max} values were observed for Cu/NBP than for Cu/NBO (Table 3), as observed in the previous TPR-1 runs. A second reduction analysis (TPR-2) was performed on the freshly reoxidized samples by TPO. The shape and position of the TPR-2 profile of Cu/NBO were markedly different from that of TPR-1, whereas TPR-2 profile of Cu/NBP showed only a limited shift toward lower temperatures than TPR-1. For both the Cu catalysts, the TPR-2 peaks appeared at lower temperatures than those of TPR-1 and the distance in temperature (peak width) of the TPR-2 peaks was lower than that of TPR-1, in particular for Cu/NBO (Figures 6 and 7 and Table 3). The lack of overlap between TPR-1 and TPR-2 suggests a mobility of the CuO species leading to a more aggregated CuO phase, even if the low reduction temperature and high extent of reduction (Table 3) suggest a low CuO phase aggregation. The mobility of the CuO species diminished by increasing the metal oxide−support interaction. This is the case of Cu/NBP, for which the shift at low temperature of T_{max} was only 32 K, without any shape modification between the TPR-2 and TPR-1 profiles. After a second TPO run, which proceeded without any appreciable variation from the first run, TPR-3 was collected on the two catalysts. In both cases, the TPR-3 profiles superposed those of TPR-2. Only for Cu/NBO, a very light loss of extent of reduction could be observed (Table 3).

Acidic Properties. The highly acidic properties of NBO and NBP surfaces are well-known and have been exploited in catalysis for many applications.[19,20,31,40,55−57] In our recent work,[25] the intrinsic and effective acidity of NBO and NBP have been studied by a multitechnique approach by titrating the surfaces with different basic probes under inert (vacuum or inert gas) or reactive (solvents of different polarity and proticity) conditions. Among the various techniques used in our previous work,[25] temperature-programmed desorption (TPD) of a basic probe has been selected for the present study.

TPD has been realized in a thermogravimetric analyzer using 2-phenylethylamine (PEA) as the probe, chosen for its high molecular mass.[25,58] The calcined NBO and NBP surfaces and relevant Cu samples were first saturated with

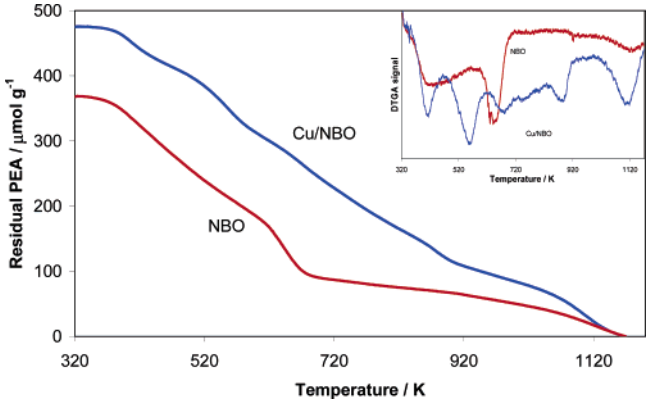

Figure 8. Thermogravimetric (TG) curves of 2-phenyl-ethylamine (PEA) desorption as a function of temperature performed at 10 K min^{-1} and first derivatives of the desorption curves (DTG) (inset) for NBO (red) and Cu/NBO (blue).

Table 4. Acidity of the Sample Surfaces Probed by TPD of PEA

	$T_{desorption}$ (K)		distribution of acid sites[a] (μequiv g^{-1})		
sample	$T_{max,1}$	$T_{max,2}$	$S_{Tmax,1}$	$S_{Tmax,2}$	$S_{T\infty}$
NBO	385.0	646.6	109 (29.6)[b]	159 (43.3)	100 (27.1)
Cu/NBO	412.3	554.6	45.8 (9.6)	118 (24.9)	311 (65.4)
NBP	438.3	670.8	194 (33.4)	321 (55.3)	65.6 (11.3)
Cu/NBP	413.8	606.1	95.3 (17.3)	203 (36.7)	255 (46.0)

[a] Sites associated with $T_{max,1}$ ($S_{Tmax,1}$), $T_{max,2}$ ($S_{Tmax,2}$), and T_∞ (temperatures higher than $T_{max,2}$; $S_{T\infty}$). [b] Percent population of acid sites is indicated in brackets.

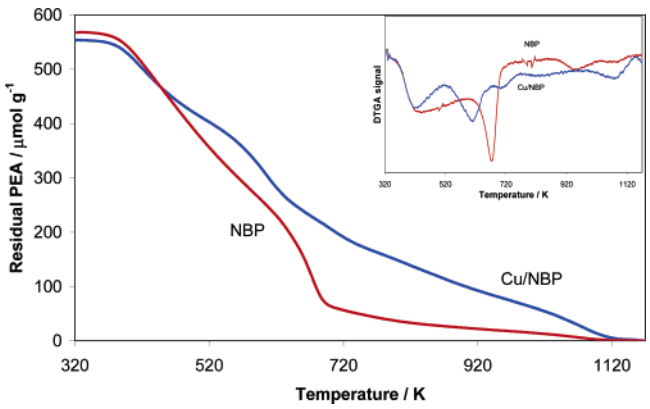

Figure 9. Thermogravimetric (TG) curves of 2-phenyl-ethylamine (PEA) desorption as a function of temperature performed at 10 K min^{-1} and the first derivatives of the desorption curves (DTG) (inset) for NBP (red) and Cu/NBP (blue).

PEA, and after complete isothermal (323 K) removal of the weakly adsorbed PEA, TPD analysis was then performed at fixed heating rate. Figures 8 (for NBO and Cu/NBO) and 9 (for NBP and Cu/NBP) comparatively show the thermogravimetric profiles of PEA desorption (residual μmol$_{PEA}$ g^{-1} vs temperature). The amount of PEA desorbed from Cu/NBO was higher than that from NBO in the whole temperature range (Figure 8). The total amount of acid sites of NBO was 630 μequiv g^{-1} when it was calcined at 673,[25] whereas the number of acid sites decreased to 368 μequiv g^{-1} when NBO was calcined at 773 K (40% of acidity decrease; Table 4). Copper could deposit over the NBO surface, forming new acid sites associated with the presence of highly dispersed copper species (Lewis acid sites). The acidity of the Cu/NBP and NBP samples was quite similar (Figure 9 and Table 4). Comparing the acidity of NBP surfaces calcined at 673[25] and 773 K (Table 4), 738 and 581 μequiv g^{-1} of sites could

(55) Abdel-Rehim, M. A.; Dos Santos, A. C. B.; Camorim, V. L. L.; Da Costa Faro, A. *Appl. Catal., A* **2006**, 305, 211−218.
(56) Védrine, J. C.; Coudurier, G.; Ouqour, A.; Pries de Oliveira, P. G.; Volta, J. C. *Catal. Today* **1996**, *28*, 3−15.
(57) Hanaoka, T.; Takeuchi, K.; Matsuzaki, T.; Sugi, Y. *Catal. Today* **1990**, *8*, 123−132.
(58) Carniti, P.; Gervasini, A.; Bennici, S. *J. Phys. Chem. B* **2005**, *109*, 1528−1536.

be determined, respectively (21% of acidity decrease). The presence of copper over the NBO and NBP supports completely modified the shape of PEA desorption curves (Figures 8 and 9). The inset of Figures 8 and 9 show the derivatives of thermogravimetric profiles (DTGA) highlighting the inflection points of the TGA curves as negative peaks. The temperatures at which the rate of PEA desorption went through a maximum (T_{max}) could be clearly detected (Table 4). Two distinct peaks ($T_{max,1}$ and $T_{max,2}$) were observed for the two supports, whereas a more complex situation was observed for the Cu samples (Table 4), whose other peaks, besides $T_{max,1}$ and $T_{max,2}$, could be guessed at higher temperatures. $T_{max,1}$ values for all the samples are lower than the boiling temperature of PEA (T_b = 471−473 K at atmospheric pressure). The amount of PEA desorbed at $T_{max,1}$ ($S_{Tmax,1}$, Table 4) could then be associated with the amount of the probe weakly bound to the acid sites. The amount of PEA desorbed at $T_{max,2}$ ($S_{Tmax,2}$, Table 4) was associated with strongly acidic sites, as already observed.[25] The remainder of PEA desorbed at higher temperatures than $T_{max,2}$ (indicated as T_∞) and was associated with very strong acid sites. The percent population of sites, $S_{Tmax,1}$ and $S_{Tmax,2}$, was lower for the Cu samples than for the relevant supports (Table 4). On the opposite, the amount of PEA desorbed at temperatures higher than $T_{max,2}$ (T_∞ and $S_{T\infty}$) was higher for the Cu catalysts than for the relevant supports.

Catalytic Activity. *N_2O Decomposition (N_2O dec).* Catalytic N_2O decomposition proceeds following a cycle that foresees (i) N_2O adsorption at the catalyst site; (ii) decomposition of N_2O, leading to the formation of nitrogen and oxygen in an adsorbed state; and (iii) oxygen desorption that frees the catalyst site from adsorbed oxygen and completes the catalytic cycle, as known from the literature.[7,592] The effective ability of N_2O decomposition of CuO phases supported over various ceramic supports[16,60] or over monoliths[61] has been well-assessed.

The N_2O decomposition tests have been completed by feeding a lean N_2O concentration in an inert atmosphere or in the presence of a large amount of oxygen. It is expected that in an oxidant atmosphere, the extent of the reaction should be lower than that in an inert atmosphere because of the presence of oxygen that does not favor the reaction course. Figure 10 shows the outlet concentration of N_2O as a function of reaction temperature for Cu/NBO and Cu/NBP in inert and oxidant atmospheres. Over Cu/NBO, the decomposition activity started at 773 K to a higher extent in an inert atmosphere and to a lower extent in an oxidant atmosphere. The activity increased with reaction temperature (residual N_2O concentration of 490 and 1110 ppm at 873 K in inert and oxidant atmospheres, respectively). The values obtained at 873 K were not steadily maintained. After about 72 min of tos (time on stream), values of 1010 ppm in inert and 1335 ppm in oxidant atmospheres were observed. This behavior could be expected because of the transformation

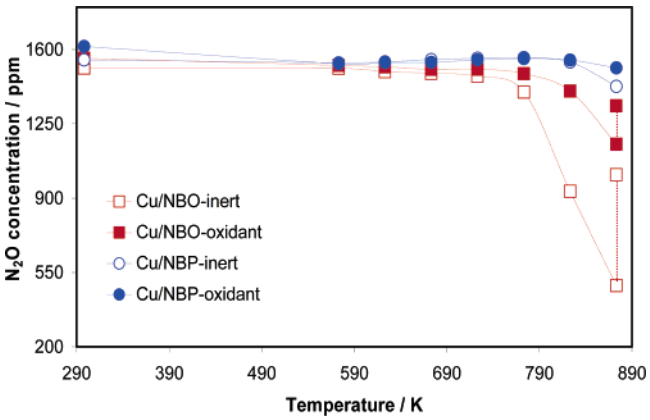

Figure 10. N_2O decomposition reaction (N_2O dec) carried out under inert (open symbols) and oxidant (filled symbols) atmospheres. Outlet N_2O concentrations as a function of reaction temperature for Cu/NBO (red) and Cu/NBP (blue).

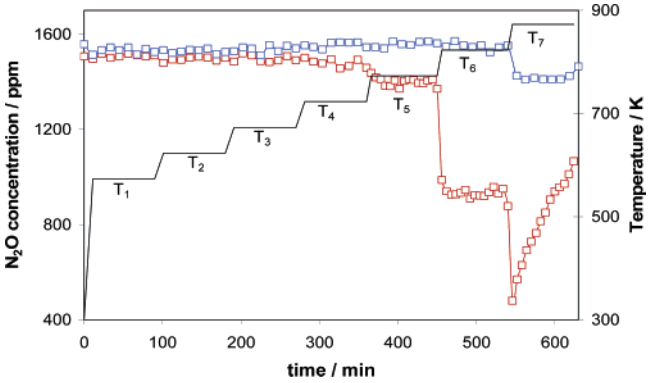

Figure 11. N_2O decomposition reaction (N_2O dec) carried out under an inert atmosphere. Temporal concentrations of N_2O for Cu/NBO (red) and Cu/NBP (blue) monitored at temperatures of 573 (T_1), 623 (T_2), 673 (T_3), 723 (T_4), 773 (T_5), 823 (T_6), and 873 K (T_7). Each plateau of temperature was maintained for 90 min.

of the TT-phase of niobia into crystalline hexagonal Nb_2O_5, which is known to start around 820 K.[31] Figure 11 shows the temporal diagram of the outlet N_2O concentration for Cu/NBO under inert atmospheric conditions for the whole temperature range investigated. It is well-evident that the Cu/NBO is stable up to temperatures below 823 K and that the activity decays with tos at 873 K. The N_2O decomposition activity of Cu/NBP was much lower but more stable than that of Cu/NBO (Figures 10 and 11). Table 5 reports the N_2O conversions obtained for both the catalysts. The differences in N_2O conversion in inert and oxidant atmospheres were very important for Cu/NBO and much lighter for Cu/NBP.

Reduction of N_2O (N_2O−SCR). The temperatures of catalytic conversion of N_2O to N_2 can be lowered by the addition of reductants.[7,62−64] Among various reductants tested, ethene has been successfully used for reducing N_2O over catalysts on the basis of dispersed CuO phases over siliceous supports of various acidity.[16] In the present investigation, the N_2O reduction by ethene has been tested over the two

(59) Chang, K. S.; Song, H.; Park, Y.-S.; Woo, J.-W. *Appl. Catal., A* **2004**, *273*, 223−231.
(60) Centi, G.; Cerrato, G.; D'Angelo, S.; Finardi, U.; Giamello, E.; Morterra, C.; Perathoner, S. *Catal. Today* **1996**, *27*, 265−270.
(61) Boissel, V.; Tahir, S.; Koh, C. A. *Appl. Catal., B* **2006**, *64*, 234−242.
(62) Corma, A.; Fornés, V.; Palomares, E. *Appl. Catal., B* **1997**, *11*, 233−242.
(63) Nobukawa, T.; Yoshida, M.; Okumara, K.; Tomishige, K.; Kunimore, K. *J. Catal.* **2005**, *229*, 374−388.
(64) Nobukawa, T.; Yoshida, M.; Kameoka, S.; Ito, S.; Tomishige, K.; Kunimori, K. *J. Phys. Chem. B* **2004**, *108*, 4071−4079.

Table 5. Main Results of the Catalytic Study of DE-NO_x Reduction and Decomposition Reactions

reaction			Cu/NBO			Cu/NBP		
N_2O-Dec		*T* (K)	773	823	873	773	823	873
	N_2O conversion (%)	inert atmosphere	7.48	38.39	67.73[a]	0	0.66	8.05
		oxidant atmosphere	4.66	9.90	25.98 [a]	3.55	3.96	6.26
N_2O-SCR		*T* (K)	773	823	873	773	823	873
	N_2O conversion (%)		9.92	25.66	59.82 [a]	4.44	10.24	17.31
	C_2H_4 conversion (%)		100	100	100	78.76	92.44	97.03
NO-SCR		*T* (K)	523	573	623	573	623	698
	NO_x[b] conversion (%)		11.67	24.56	18.76	8.33	10.97	6.79
	C_2H_4 conversion (%)		19.32	77.94	98.96	6.66	16.37	42.06

[a] Calculated at the attainment of temperature. [b] $NO_x = NO + NO_2$.

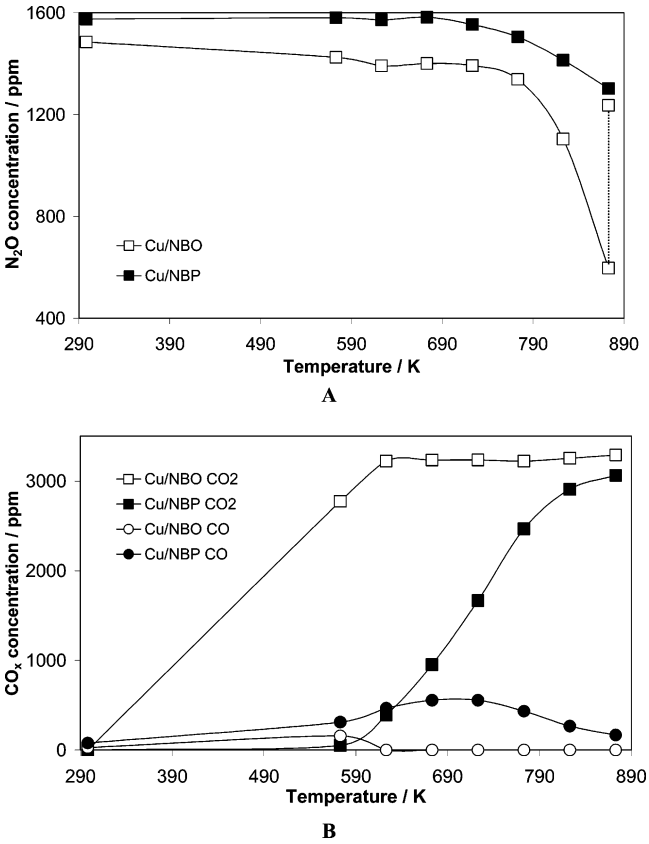

Figure 12. Selective catalytic reduction of N_2O (N_2O-SCR). Profiles of (A) N_2O and (B) CO and CO_2 concentrations as a function of reaction temperature for Cu/NBO (open symbol) and Cu/NBP (filled symbol). The feed concentration (298 K) is also indicated.

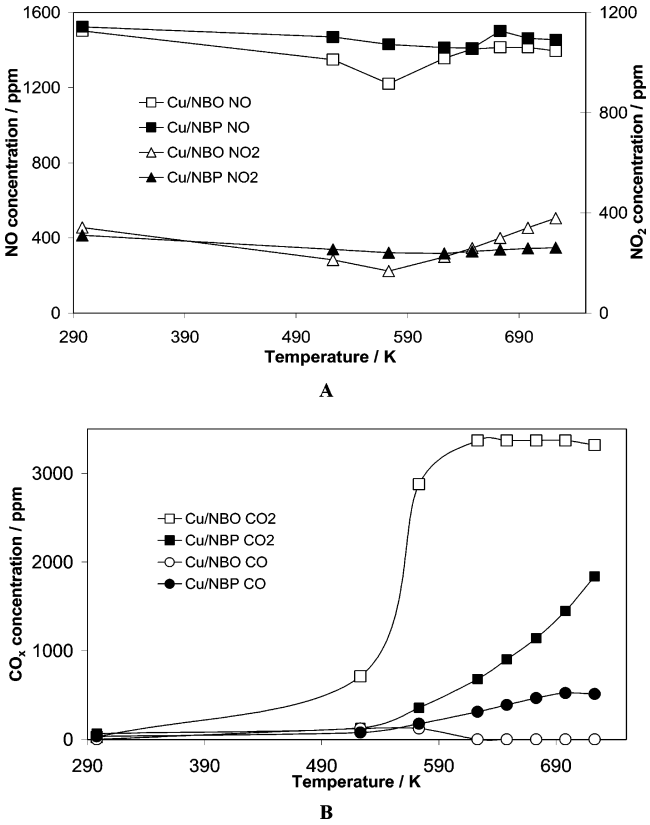

Figure 13. Selective catalytic reduction of NO ($NO-SCR$). Profiles of (A) NO and NO_2 and (B) CO and CO_2 concentrations as a function of reaction temperature for Cu/NBO (open symbol) and Cu/NBP (filled symbol). The feed concentration (298 K) is also indicated.

studied Cu/NBO and Cu/NBP catalysts. The obtained concentration profiles of reagents and products as a function of reaction temperature are shown in panels A and B of Figure 12. Selected results of N_2O and C_2H_4 conversion have been reported in Table 5. The onset of N_2O reduction was around 773 K; there was 10 and 4% conversion for Cu/NBO and Cu/NBP, respectively. At 873 K, the outlet N_2O concentration corresponded to 60% of N_2O conversion to N_2 for Cu/NBO and only 17% for Cu/NBP. As indicated above, Cu/NBO was not stable at the highest reaction temperature (873 K); the obtained stable outlet N_2O concentration was even higher than that at 823 K (Figure 12). C_2H_4 was completely converted to CO_2 with very poor amount of CO formation over Cu/NBO, whereas not complete C_2H_4 conversion was obtained over Cu/NBP, with formation of an appreciable amount of CO in the 590−790 K interval. The behavior presented in the Figures 12 and 13 accounts for a high SCR selectivity of Cu/NBP, which is active at very high temperatures, and a poor SCR selectivity of Cu/NBO. The high N_2O conversions observed over Cu/NBO at the highest reaction temperatures (773−873 K) could be due to N_2O decomposition rather than N_2O reduction, because the poor presence of C_2H_4. In any case, the presence of C_2H_4 is beneficial for the N_2O conversion to N_2. In fact, comparing the N_2O-dec (carried out in oxidant atmosphere) with N_2O-SCR, more than two times higher N_2O conversion for the N_2O-SCR was obtained (Table 5).

Reduction of NO (NO−SCR). CuO is among the most interesting transitional oxides for the reduction of NO by hydrocarbon reductants, with numerous papers and reviews accounting for its promising activity.[8,13,14,62,63,65,66] The nature and properties (in particular the acidity) of the support seem to be decisive for the activity and selectivity of the

(65) Pârvulescu, V. I.; Grange, P.; Delmon, B. *Catal. Today* **1998**, *46*, 233−316.
(66) Traa, Y.; Burger, B.; Weitkamp, J. *Microporous Mesoporous Mater.* **1999**, *30*, 3−41.

CuO phase.[11,16] As expected, the NO−SCR activity of Cu/NBO and Cu/NBP greatly differed. Panels A and B of Figure 13 show the concentration profiles of reagents and products as a function of temperature. The NO outlet concentration first decreased, passed through a minimum, and then increased with temperature, whereas an S-shaped curve was obtained for the CO_2 formation (and C_2H_4 disappearance). The minimum NO concentration corresponded to 25% NO conversion, at 573 K (Table 5). Cu/NBP showed poor activity toward NO reduction to N_2 as well as toward C_2H_4 conversion to CO_2 (Table 5). Once again, the superior activity of Cu/NBO in reactions involving NO_x emerged. This could indicate the active role of the oxide support in the NO_x reactions, in agreement with the recent findings of the literature indicating the bifunctional action of supported metal oxides over oxide supports.

Conclusions

The main observed differences between the dispersed copper oxide phases on the two niobium-based support materials are related to the interfacial electronic interactions of the metal oxide with support that influenced the redox properties and mobility of the supported phase. The activity of the catalysts, tested in NO_x decomposition and reduction reactions, was lower for CuO supported over niobium phosphate than for CuO supported on niobic acid. The latter system showed comparable activity with the most conventional catalysts of copper oxide supported on siliceous supports.[16,53] Some considerations can be derived from this study that points out the influence of nature and intrinsic properties (ionicity and covalency) of the support on the physicochemical and catalytic properties of the dispersed CuO phase. Could it be possible to modulate the properties of supported oxides by controlling the electronic properties of the dispersing supports?

Supporting Information Available: XPS experimental data; temperature-programmed reduction profiles; absorbance FT−IR spectra. This material is available free of charge via the Internet at http://pubs.acs.org.

CM062503V